ACS OMEGA

http://pubs.acs.org/journal/acsodf

Article

Adsorption of Greenhouse Decomposition Products on Ag_2O-SnS_2 and $CuO-SnS_2$ Surfaces

Wei Gong, Jingcheng Liu,* Yingang Gui,* and Heqing Huang

Cite This: *ACS Omega* 2022, 7, 21043−21051

Read Online

ACCESS | Metrics & More | Article Recommendations

ABSTRACT: In this paper, based on density functional theory, the adsorption mechanism and gas sensitivity of Ag_2O/CuO-modified SnS_2 were analyzed. The results were analyzed according to the adsorption energy, total density of states, partial density of states, and frontier molecular orbital theory. The results show that the adsorption of all gas molecules is exothermic. NH_3, Cl_2, and C_2H_2 gases are chemisorbed on the modified SnS_2 surfaces. After gas adsorption, the energy gap of the base changes by more than 10%, which fully shows that the conductivity changes greatly after gas adsorption, which can be reflected in the macroscopic resistance change. Ag_2O-SnS_2 is suitable as a gas sensor for NH_3 gas sensors in terms of moderate adsorption distance, large adsorption energy, charge transfer, and frontier molecular orbital theory, while $CuO-SnS_2$ is more suitable as a C_2H_2 gas sensor.

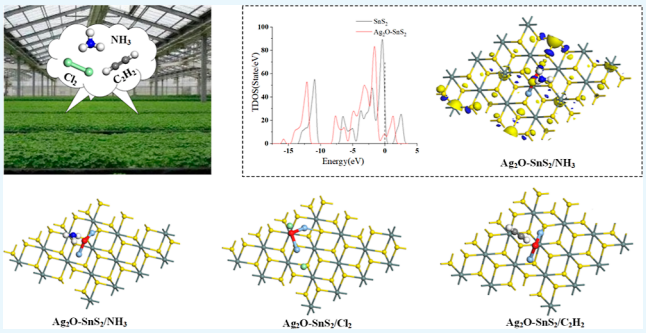

1. INTRODUCTION

Greenhouse cultivation is favored by more and more farmers for advancing or delaying the planting season, increasing planting density, and bringing greater economic benefits.[1,2] With the continuous improvement of cultivation technology, the scale of greenhouse cultivation is becoming larger and larger.[3,4] However, because of the relative isolation of the internal and external environment of the greenhouse, temperature, humidity, moisture, and other factors are relatively stable in the hut, it is easy for gases to accumulate in the hut, which may endanger crop life at a certain concentration.[5] Therefore, it is necessary to provide gas sensors that can detect the gas content in the greenhouse to achieve the effect of adjusting the amount and type of the gas content in the greenhouse in time. Besides, gas sensors are easy to popularize because of their low cost, which facilitates the achievement of certain economic benefits.[6,7] In this paper, NH_3, Cl_2, and C_2H_2 produced in the greenhouse are the main representative gases of the greenhouse through the analysis of these three gases carried out in this research.[8,9]

In recent years, SnS_2-based materials have been widely used as gas sensors in the industry due to their large specific surface area and abundant pore structure.[10] Compared with carbon nanotubes, SnS_2 has stronger oxidation resistance, high-temperature stability, and smaller dependence, so SnS_2 is more suitable for gas detection than carbon nanotubes.[11,12] Therefore, it has become one of the most promising materials in high-temperature and high-pressure environments.[13,14] However, the reaction of intrinsic SnS_2 to some inert gases is limited, such as CH_4, C_2H_2, and H_2. Fortunately, metal doping modification can adjust the energy gap of the gas-sensing material, thus changing the conductivity of the sensor upon gas adsorption, resulting in improved detection accuracy and adsorption capacity of these gases.[15] Pd, Pt, Au, Ag, Ni, and Co are often used to improve the sensitivity, measurement accuracy, selectivity, and reaction recovery time of gas response. However, the strong surface activity of metal atoms makes the gas sensor easily susceptible to oxidation during a long time operation, which significantly reduces the sensor's stability. Metal oxides, such as Ag_2O and CuO, are the most widely used surface modifications, which show good chemical stability. Salvatore found that SnS_2/SnO_{2-x} mixed phases showed outstanding gas-sensing performance to NH_3.[16] Hao fabricated SnS_2/SnO_2 sensors that exhibited ultrahigh response toward 1 ppm NO_2 at 100 °C, roughly 10.2 times higher than that of pure SnS_2 nanoflowers.[17]

In this paper, Ag_2O and CuO-modified SnS_2 (TMO-SnS_2) are proposed as promising greenhouse gas-sensing materials, which can be used to monitor the change in indoor gas concentrations.[18] First, the structure of TMO-SnS_2 is optimized to obtain highly stable structures. Then, the most stable structure is used to analyze its adsorption properties to NH_3, Cl_2, and C_2H_2.[19,20] The modification and gas-sensing mechanism of

Received: March 25, 2022
Accepted: May 24, 2022
Published: June 6, 2022

TMO-SnS_2 are also described. By analyzing the structure optimization, adsorption energy, energy band structure, density of states, and charge transfer, it is found that the modified SnS_2 sensor shows a high gas-sensing response.[21] The optimal site of gas adsorption can be found through structural optimization analysis, and the model can be used as the model of gas adsorption to analyze the gas-sensing response results. Based on this model, the reaction types and reaction intensities of gas adsorption are analyzed by the adsorption distance, adsorption energy, and charge transfer again through the density of states analysis and frontier molecular orbital theory analysis to further explore the mechanism of gas adsorption afterward, in which the density of states analysis shows that the gas adsorption type and reaction intensity can be determined through the analysis of the frontier molecular orbital theory, which shows that the energy gap of the gas changes and it changes to reflect the conductivity of the gas charge transfer. This study provides a new method for monitoring the concentration of indoor greenhouse gases.[22]

2. COMPUTATIONAL DETAILS AND METHODS

All calculations were carried out based on density functional theory (DFT).[23,24] A periodic boundary model was adopted to avoid the interaction between adjacent cells. The vacuum thickness of the (1 0 1) lattice plane was set to 18.0 Å.[25,26] The Brillouin zone *k*-point sampling was sampled by 3 × 3 × 1. The electron exchange and correlation energy were calculated by the GGA, and the interaction effect of electrons was treated by the PBE function, whereas a double numerical basis with polarization (DNP) was used.[27,28] The convergence criterion for energy and force was set as 10^{-5} Ha and 2 × 10^{-3} Ha/Å, respectively, and the charge density convergence accuracy of the self-consistent field was 1 × 10^{-6} Ha.[29,30]

The adsorption energy E_{ads} shows the change in total energy in the process of adsorption, which can be calculated by eq 1.[31,32] In this formula, $E_{suf/gas}$, E_{suf}, and E_{gas} represent the total energy of the system after the gas molecule's adsorption on TMO-SnS_2, the total energy of the TMO-SnS_2 surface, and the total energy of individual gas molecules before adsorption, respectively.[33,34]

$$E_{ads} = E_{suf/gas} - E_{suf} - E_{gas} \quad (1)$$

The electron density distribution was calculated by Mulliken population analysis. The charge transfer Q in the adsorption process was obtained by eq 2, where Q_{iso} and Q_{ads} are the total charges of isolated gas and adsorbed gas molecules.[35,36] $Q > 0$ means that electrons transfer from gas molecules to the surface of TMO-SnS_2.[37,38]

$$Q = Q_{ads} - Q_{iso} \quad (2)$$

The energy gap of the molecular orbital can be calculated by the energy levels of the highest occupied molecular orbital (HOMO) and the lowest occupied molecular orbital (LUMO), defined as eq 3.[39−42] It determines the probability of charge movement in the adsorption system composed of gas molecules and the TMO-SnS_2 surface.[43−46] The narrower the gap, the lower the energy required for electrons to transfer from the valence band to the conduction band.[47,48]

$$E_g = |E_{LUMO} - E_{HOMO}| \quad (3)$$

3. RESULTS AND DISCUSSION

3.1. Structure of SnS_2 and TMO-SnS_2 Surfaces. As shown in Figure 1, the gas molecular structure and intrinsic SnS_2 structure are optimized. C_2H_2 and Cl_2 are linear gas molecules, while NH_3 has a three-dimensional tetrahedral structure. The length of the Cl−Cl bond is 2.024 Å, and the lengths of the C−H bond and C−C bond in the C_2H_2 molecule are 1.071 and 1.211 Å, respectively. The N−H bond angle of the NH_3 molecule is 105.35°. The symmetrical N−H bonds of the NH_3 molecule ensure its chemical stability. SnS_2 with a perfect crystal structure is shown in Figure 1d. The two-dimensional structure is beneficial in improving the adsorption performance.[49,50] The S−Sn bond length of 2.611 Å is appropriate for structural stability, and the axial and circumferential distances are close to this value. In general, SnS_2 is a suitable material for gas adsorption.

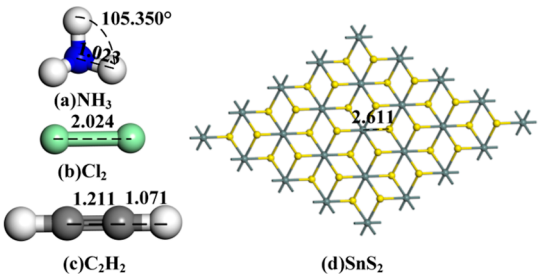

Figure 1. (a) NH_3 molecule, (b) Cl_2 molecule, (c) C_2H_2 molecule, and (d) SnS_2 molecule. The distance is in Å.

Figure 2 shows the most stable doping structure of Ag_2O and CuO-modified SnS_2. The distribution of SnS_2 atoms shows centrosymmetry. The Ag−S bond length (2.406 Å) is slightly shorter than the O−S bond length (3.513 Å), which is consistent with the bond length between heavy metals. This phenomenon illustrates a strong interaction between the Ag and S atoms. The formation energy is −1.626 eV, which confirms the good stability of the interacting structure. The O−S bond length of -doped species is 1.593 Å, which is slightly shorter than the Cu−S bond length of 3.633 Å. It signifies the strong interaction between the O and S atoms. The adsorption energy reaches −1.713 eV, which proves that the structure of CuO−SnS_2 is extremely stable. Based on the Mulliken population, 0.063 *e* electrons and 0.054 *e* electrons transfer to SnS_2 from Ag_2O and CuO as electron donors, respectively. This redistribution of charge results in a change in the conductivity of the doping system.

The density of states was analyzed to further study the interaction mechanism of Ag_2O and CuO-modified SnS_2, as shown in Figure 3. After Ag_2O and CuO doping on the SnS_2 surface, the total density of states (TDOS) changes significantly in the range of −2 to −5 eV and −1 to 1 eV. The TDOS of TMO-SnS_2 consists mainly of 3p orbitals of the S atom. According to the analysis of the partial density of states (PDOS), the 3p orbital of S and the 4d orbital of Ag overlap significantly around −4 eV. The orbital hybridization occurs when the Ag atom interacts with the S atom, indicating that the interaction of SnS_2 with Ag_2O mainly comes from the S atom of the SnS_2. The 3p orbital of S and the 2p orbital of O shapes overlap significantly around −5 eV. The orbital hybridization occurs when the O atom interacts with the S atom, indicating that the interaction between SnS_2 and CuO atom mainly comes from the S atom and the O atom.

3.2. NH_3, Cl_2, and C_2H_2 Adsorption on TMO-SnS_2 Surfaces. To study the adsorption characteristics of NH_3, Cl_2, and C_2H_2 on TMO-SnS_2, the gas molecules were adsorbed on the TMO-SnS_2 surface from different directions and angles. The most stable gas adsorption structures on Ag_2O and CuO−

https://doi.org/10.1021/acsomega.2c01828
ACS Omega 2022, 7, 21043−21051

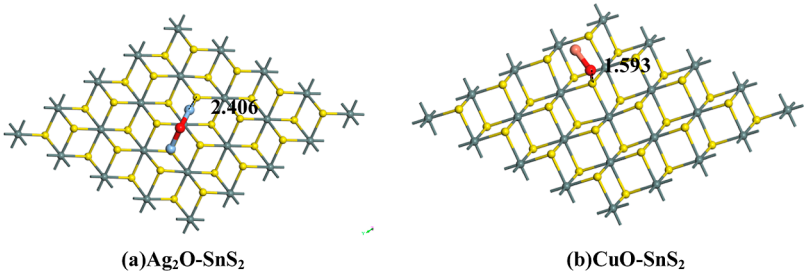

Figure 2. Most stable structure of the (a) Ag_2O-SnS_2 surface and (b) $CuO-SnS_2$ surface. The distance is in Å.

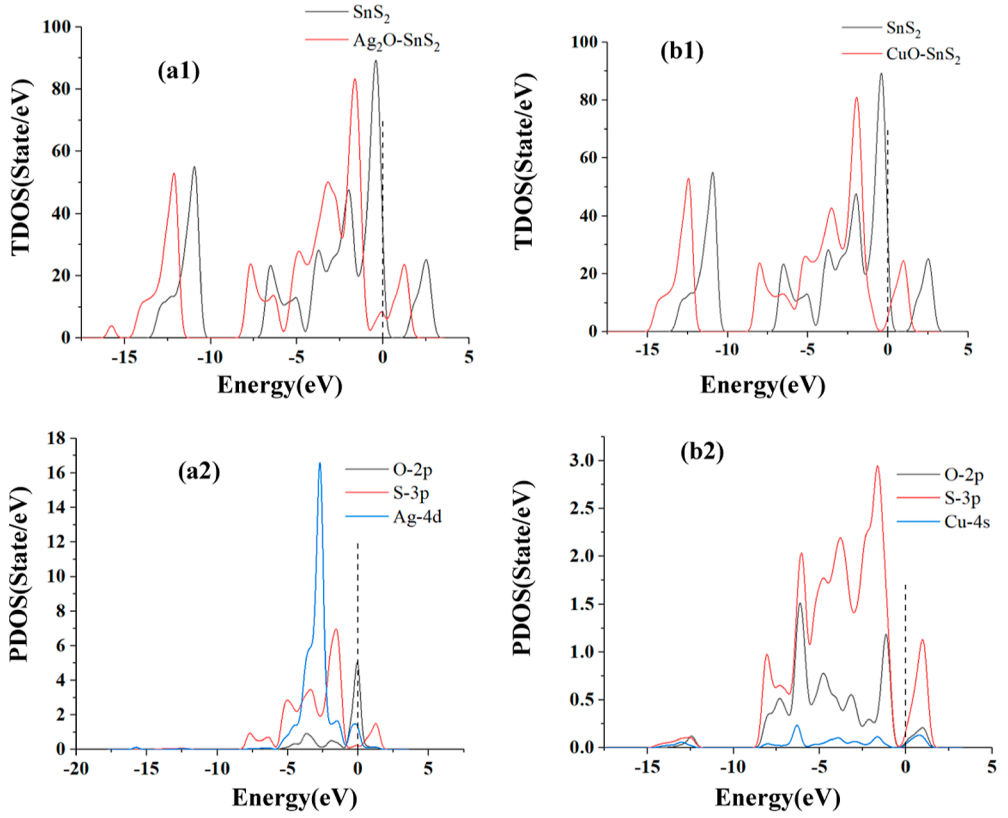

Figure 3. TDOS and PDOS of before and after gas molecule adsorption on (a) Ag_2O-SnS_2 and (b) $CuO-SnS_2$.

SnS_2 surfaces are shown in Figures 3 and 5, respectively. The density of states, band structure, and molecular orbital of the adsorption process were analyzed by taking the most stable adsorption structure that has the largest adsorption energy.

3.2.1. Gas Adsorption on the Ag_2O-SnS_2 Surface. The adsorption distances of NH_3, Cl_2, and C_2H_2 on Ag_2O-SnS_2 are 1.754, 1.724, and 1.905 Å, respectively. The structures of NH_3 and C_2H_2 gas molecules stay intact in the adsorption process, but the Cl−Cl bond breaks in the adsorption process of Cl_2. It can be seen that the adsorption distance of NH_3, Cl_2, and C_2H_2 by $Ag-SnS_2$ is relatively moderate, which is conducive to the subsequent desorption, making the recycling of sensing material and improving the sensitivity of the gas sensor. In the adsorption process of NH_3 gas, the H atom is absorbed on the O atom; it can be speculated that there is a chemical bond between the H atom and the O atom because when N atoms and H atoms combine to form NH_3, N atoms have a larger radius and are less likely to lose electrons and gain electrons, while H atoms have a smaller radius and possess more ability to lose electrons. As can be seen from the previous paper, in the doping process of Ag_2O on SnS_2, the O atom gains electrons, thus making the O atom show more electrons to bond with the H atom that lost electrons. This is the mechanism in which the H atom approaches Ag_2O-SnS_2, while the N atom is far away from the Ag_2O-SnS_2. It can be seen that the adsorption of NH_3, Cl_2, and C_2H_2 by Ag_2O-SnS_2 belongs to chemical adsorption. In addition, when Ag_2O-SnS_2 adsorbed Cl_2 gas, the chemical bond between Cl−Cl was broken due to excessive adsorption energy and charge transfer, so the adsorption was not reversible. After adsorption, the modified SnS_2 substrate was in a state that could not be reused. The adsorption of the other two gases can be desorbed for recycling applications.

Figure 5 shows the TDOS and PDOS before and after adsorption of NH_3, Cl_2, and C_2H_2 by Ag_2O-SnS_2, where dotted lines represent the Fermi levels. It can be seen in Figure 5a1−c1 that the peak value of the TDOS shifts significantly to the left after adsorption, making it continuous at the Fermi level. In Figure 5a1,b1, it can be seen that Ag_2O-SnS_2 generates a new peak value at −5.0 to −7.5 eV due to the hybridization of Ag 4d, N 2p, O 2p, and H 1s in the adsorption process of NH_3. In Figure 4a2,b2, it can be seen that during the adsorption of Cl_2, Ag_2O-SnS_2 produced a new peak due to the hybridization of Ag 4d, O

https://doi.org/10.1021/acsomega.2c01828
ACS Omega 2022, 7, 21043−21051

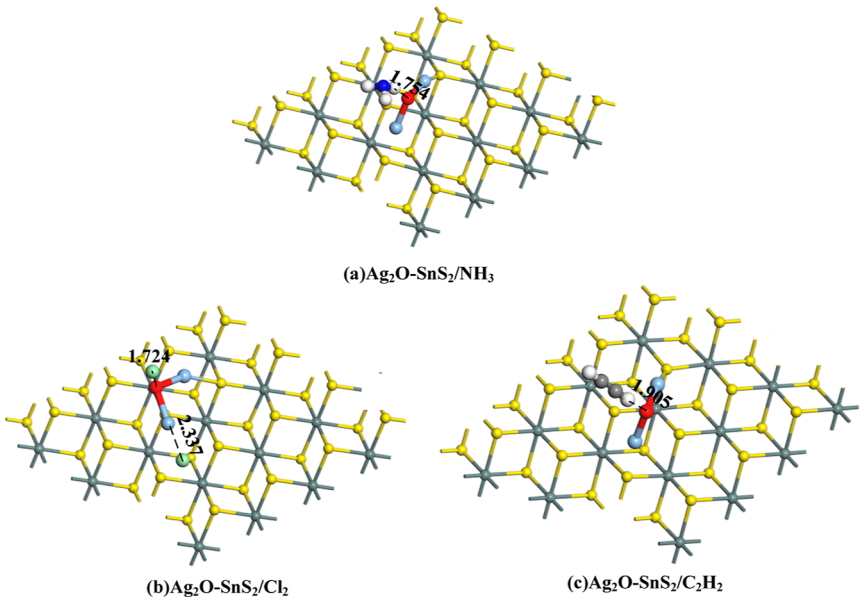

Figure 4. Most stable structures of gas molecules on Ag_2O-SnS_2: (a) Ag_2O-SnS_2/NH_3, (b) Ag_2O-SnS_2/Cl_2, and (c) Ag_2O-SnS_2/C_2H_2. The distance is in Å.

2p, and Cl 3p at −0 to −5.0 eV. In Figure 5a3−b3, Ag_2O-SnS_2 generates a new peak due to the hybridization of Ag 4d, C 2p, O 2p, and H 1s at −5.0 to −10.0 eV during the adsorption of C_2H_2. The generation of the new peak value makes the chemisorption more stable, and the larger the overlapping peak value, the stronger the chemical interaction. In Figure 5b1, it can be seen that the peak value of the overlap is very large when Ag_2O-SnS_2 adsorbs Cl_2, which also confirms that the adsorption chemistry of Cl_2 is very strong, leading to the rupture of the Cl−Cl chemical bond. However, Ag_2O-SnS_2 has no new peak value for C_2H_2, which also confirms that the chemical adsorption of C_2H_2 is too weak, making C_2H_2 desorb easily.

The adsorption parameters of Ag_2O-SnS_2 for the three gases are shown in Table 1, including the adsorption distance, adsorption energy, and charge transfer. The adsorption energies of the NH_3, Cl_2, and C_2H_2 adsorption structures are −0.463, −0.742, and −0.354 eV, in which the negative adsorption energy means that the reaction can be spontaneous. Therefore, Ag_2O-SnS_2 has moderate adsorption energy for NH_3, Cl_2, and C_2H_2, which will not be too large for hard desorption nor too small to detect these three gases due to low adsorption energy. The charge transfer of the three adsorption structures during the adsorption process is 0.138 *e*, −0.176 *e*, and 0.013 *e*, in which the negative charge transfer represents the transfer of electrons from gas to Ag_2O-SnS_2, while the positive charge transfer represents the transfer of electrons from Ag_2O-SnS_2 to gas molecules.

3.2.2. Gas Adsorption on the CuO−SnS$_2$ Surface. As the adsorption structures shown in Figure 6, the distances of NH_3, Cl_2, and C_2H_2 on the $CuO-SnS_2$ substrate are 2.266, 2.168, and 2.277 Å, respectively. It can be seen that the structures of the three gas molecules and $CuO-SnS_2$ are kept intact when gas molecules are adsorbed on the surface of $CuO-SnS_2$. The adsorption distance, adsorption energy, and charge transfer of the three gas adsorption structures are listed in Table 2. In the adsorption process of $CuO-SnS_2$ toward NH_3 gas, H atoms are close to the substrate, while N atoms stay far away. The large adsorption distance of $CuO-SnS_2$ to NH_3 can be inferred as physical adsorption. In the adsorption process of Cl_2 gas, the Cl atom closes to the Cu atom because of the abundant electronegativity of the Cl atom and the abundant positive charge of the Cu atom. In the adsorption process of C_2H_2 gas, the H atom is absorbed on the O atom of CuO. This is because when C and H combine to form C_2H_2, C has a larger radius and is less likely to lose electrons and gain electrons, while H has a smaller radius and is more likely to lose electrons. The adsorption energies of NH_3, Cl_2, and C_2H_2 gases are −0.327, −0.925, and −0.299 eV, respectively. Charge transfer is 0.046 e, −0.115 e, and −0.072 e, respectively.

Figure 7 shows the TDOS and PDOS before and after $CuO-SnS_2$ adsorbs NH_3, Cl_2, and C_2H_2, where dotted lines represent Fermi energy levels. It can be seen in Figure 7a1−c1 that the peak value of the total density of states shifts significantly to the left after adsorption, making it continuous at the Fermi level. As can be seen from Figure 7a1,b1, $CuO-SnS_2$ generated a new peak value at −5.0 to −7.5 eV due to the hybridization of Cu 4s, N 2p, O 2p, and H 1s in the adsorption process of NH_3. In Figure 7a2,b2, it can be seen that $CuO-SnS_2$ generates a new peak value due to the hybridization of Cu 4s, O 2p, and Cl 3p at −2.5 to −5.0 eV during the adsorption of Cl_2. In Figure 7a3−b3, it can be seen that $CuO-SnS_2$ generates a new peak due to the hybridization of Cu 4s, C 2p, O 2p, and H 1s at −7.5 to −10.0 eV during C_2H_2 adsorption.

The adsorption parameters of $CuO-SnS_2$ for the three gases are shown in Table 1, including adsorption distance, adsorption energy, and charge transfer. The adsorption energies of the three adsorption structures are −0.327, −0.925, and −0.299 eV in order, in which the negative adsorption energy means that the reaction can be spontaneous. Therefore, it can be seen that $CuO-SnS_2$ has moderate adsorption energy for NH_3, Cl_2, and C_2H_2 and does not generate large adsorption energy so that NH_3, Cl_2, and C_2H_2 gases cannot be desorbed nor can it detect these three gases due to low adsorption energy. The charge transfer of the three adsorption structures is 0.046 e, −0.115 e, and 0.072 e respectively.

3.3. Molecular Orbital Theory Analysis of Gas Adsorption on Ag_2O-SnS_2 and $CuO-SnS_2$. The behavior of system electrons in the adsorption process was analyzed by frontier molecular orbital theory, and HOMO and LUMO after

https://doi.org/10.1021/acsomega.2c01828
ACS Omega 2022, 7, 21043−21051

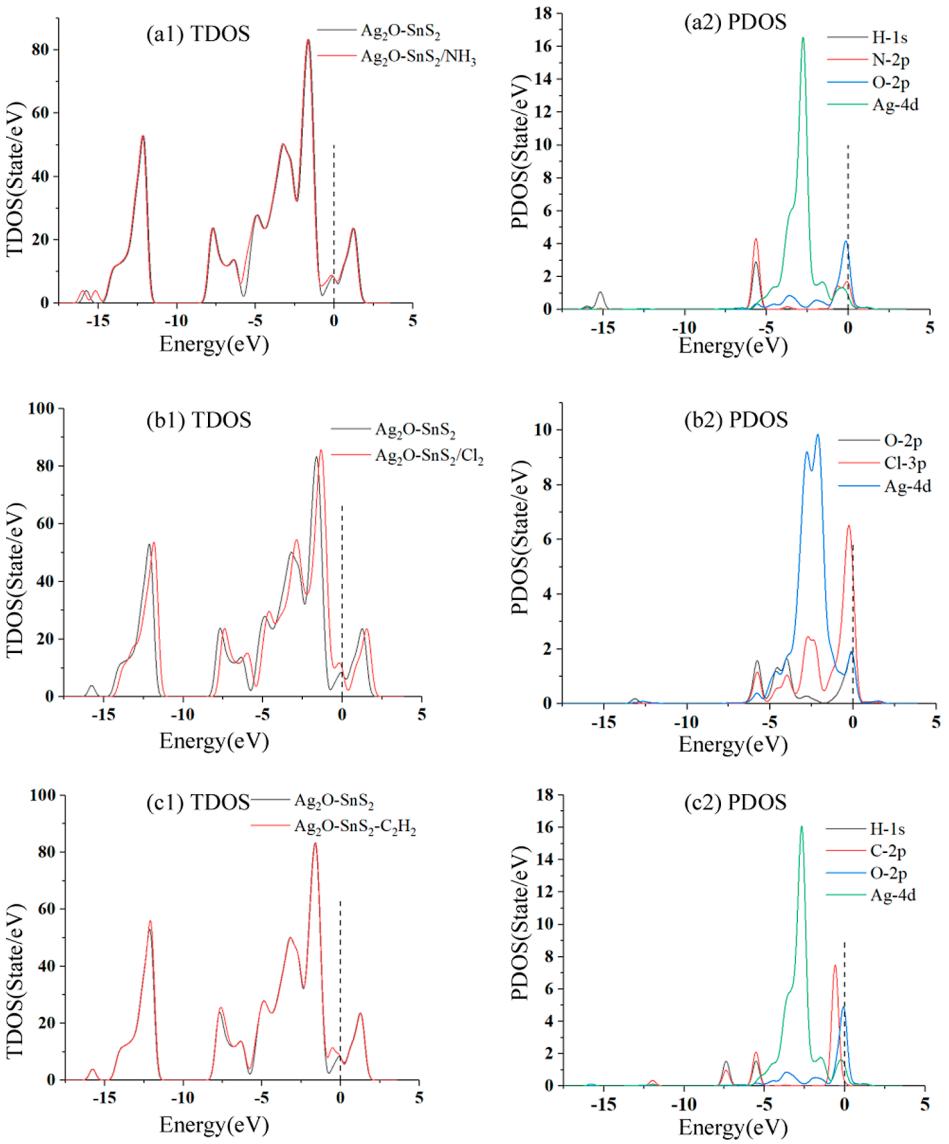

Figure 5. TDOS and PDOS of before and after gas molecule adsorption on Ag_2O-SnS_2.

Table 1. Adsorption Parameters of Gas Molecules on Ag_2O-SnS_2

configuration	structure	d (Å)	E_{ads} (eV)	Q_T (e)
Ag_2O-SnS_2/NH_3	Figure 4a	1.754	−0.463	0.138
Ag_2O-SnS_2/Cl_2	Figure 4b	1.724	−0.742	−0.176
Ag_2O-SnS_2/C_2H_2	Figure 4c	1.905	−0.354	−0.013

adsorption of NH_3, Cl_2, and C_2H_2 gases were obtained, as shown in Figures 8 and 9. Since the HOMO is denser, the system is more likely to give away electrons, whereas since LUMO is less dense, the electron affinity is stronger, and the size of the energy gap can be an indicator of a system's conductivity. The increase in metal oxide doping can reduce E_g and thus increase the conductivity.

Before Ag_2O-SnS_2 adsorbs gas, HOMO is mainly distributed on Ag, indicating that the Ag atom provides electrons as electron donors and is also the active site that can provide adsorption sites for NH_3, Cl_2, and C_2H_2 gases. After adsorption of NH_3, Cl_2, and C_2H_2 gases, HOMO becomes more concentrated on Ag, while LUMO becomes more uniform. The band gaps of Ag_2O-SnS_2 adsorbed by the three gases are 0.016, 0.025, and 0.019 eV, as shown in Table 3, respectively. The HOMO and LUMO distribution on the Ag atom after Ag_2O-SnS_2 is adsorbed by NH_3 is very small, indicating that the electron distribution of the system is more uniform. The moderate band gap also indicates that Ag_2O-SnS_2 is more suitable for the gas sensor of NH_3.

HOMO is mainly distributed on Cu before $CuO-SnS_2$ adsorbs gas, indicating that the Cu atom provides electrons as electron donors and is also the active site to provide adsorption sites for NH_3, Cl_2, and C_2H_2 gases. After adsorption of NH_3, Cl_2, and C_2H_2 gases, HOMO changes become more concentrated on Cu, while LUMO becomes more uniform. Moreover, the change is most obvious after the adsorption of Cl_2 gas. It can be seen from the above that this is due to the strong interaction of molecular orbitals after $CuO-SnS_2$ adsorption on Cl_2, which makes HOMO and LUMO more homogeneous. In addition, there is almost no LUMO on CuO, which is also due to the strong chemical interaction between CuO and Cl_2 gas, making CuO relatively stable. However, when $CuO-SnS_2$ adsorbs C_2H_2, LUMO still exists in large quantities on CuO, which is caused by the weak interaction between C_2H_2 and CuO. As shown in Table 4, the band gaps of $CuO-SnS_2$ adsorbed by the

https://doi.org/10.1021/acsomega.2c01828
ACS Omega 2022, 7, 21043−21051

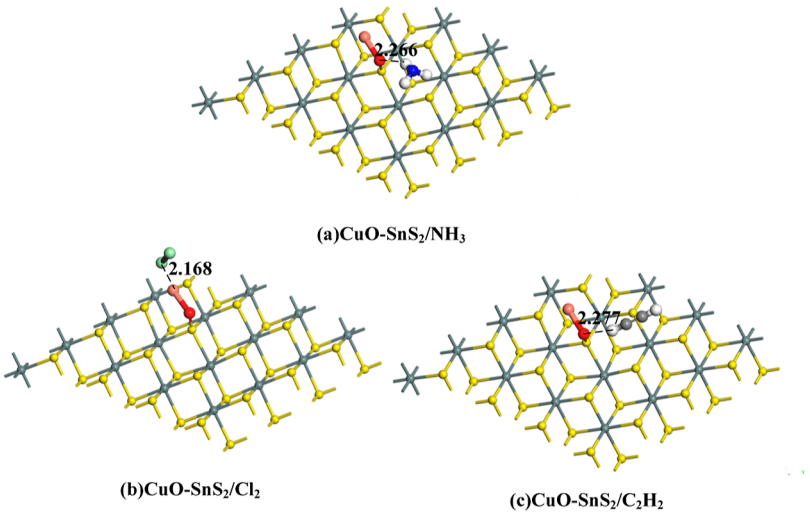

Figure 6. Most stable structures of gas molecules on CuO−SnS_2. (a) CuO−SnS_2/NH_3, (b) CuO−SnS_2/Cl_2, (c) CuO−SnS_2/C_2H_2. The distance is in Å.

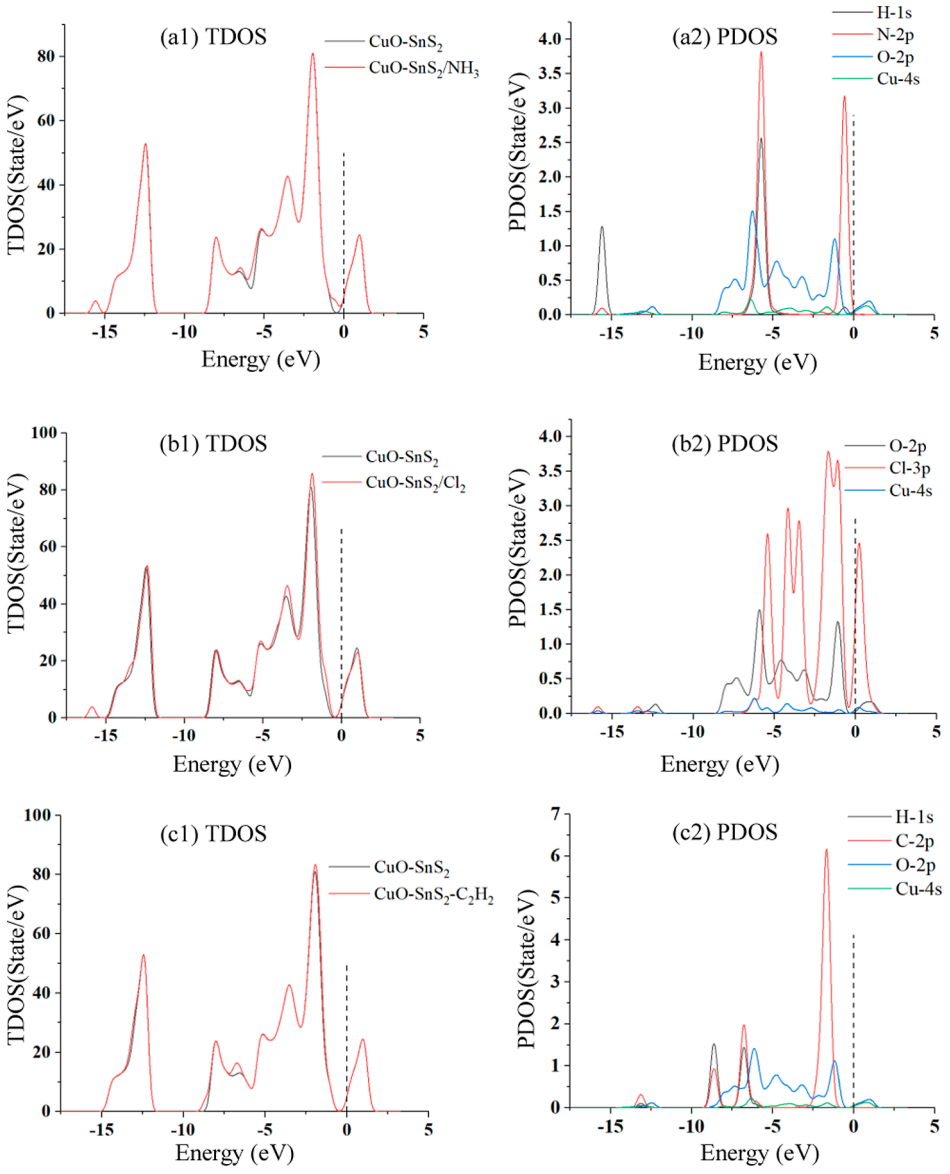

Figure 7. TDOS and PDOS of before and after gas molecule adsorption on CuO−SnS_2.

https://doi.org/10.1021/acsomega.2c01828
ACS Omega 2022, 7, 21043−21051

Table 2. Adsorption Parameters of Gas Molecules on CuO−SnS_2

configuration	structure	d (Å)	E_{ads} (eV)	Q_T (e)
CuO−SnS_2/NH_3	Figure 6a	2.266	−0.327	0.046
CuO−SnS_2/Cl_2	Figure 6b	2.168	−0.925	−0.115
CuO−SnS_2/C_2H_2	Figure 6c	2.277	−0.299	0.072

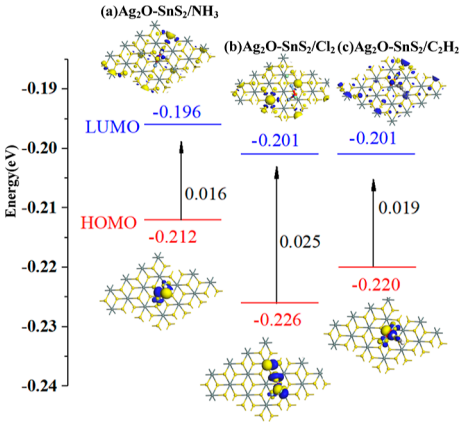

Figure 8. HOMO and LUMO of Ag_2O−SnS_2 and adsorption systems.

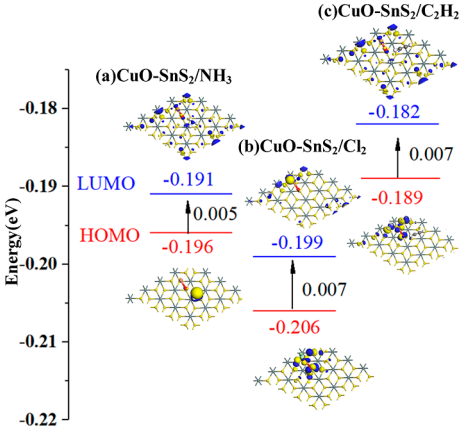

Figure 9. HOMO and LUMO of CuO−SnS_2 and adsorption systems.

Table 3. Energy of HOMO, LUMO, and the Energy Gap of Ag_2O−SnS_2 and Adsorption Systems

configuration	structure	E_{HOMO} (eV)	E_{LUMO} (eV)	E_g (eV)
Ag_2O−SnS_2/NH_3	Figure 8a	−0.212	−0.196	0.016
Ag_2O−SnS_2/Cl_2	Figure 8b	−0.226	−0.201	0.025
Ag_2O−SnS_2/C_2H_2	Figure 8c	−0.220	−0.201	0.019

Table 4. Energy of HOMO, LUMO, and the Energy Gap of CuO−SnS_2 and Adsorption Systems

configuration	structure	E_{HOMO} (eV)	E_{LUMO} (eV)	E_g (eV)
CuO−SnS_2/NH_3	Figure 9a	−0.196	−0.191	0.005
CuO−SnS_2/Cl_2	Figure 9b	−0.206	−0.199	0.007
CuO−SnS_2/C_2H_2	Figure 9c	−0.189	−0.182	0.007

three gases are 0.005, 0.007, and 0.007 eV, respectively. The HOMO and LUMO distribution on Cu atoms after CuO−SnS_2 is adsorbed by C_2H_2 is very small, indicating that the electron distribution of the system is more uniform. The moderate band gap also indicates that CuO−SnS_2 is more suitable for the C_2H_2 gas sensor.

4. CONCLUSIONS

In this paper, the adsorption properties of Ag_2O−SnS_2 and CuO−SnS_2 for NH_3, Cl_2, and C_2H_2 gases were calculated based on first principles. First, the most stable structures of the Ag_2O and CuO modification on SnS_2 were analyzed with various doping sites. The introduction of Ag_2O and CuO metal oxide doping increases the conductivity of SnS_2-based materials. Then, the interaction between Ag_2O and CuO-modified SnS_2 and gas molecules was comprehensively understood by the adsorption structure, the density of states, and frontier molecular orbital theory. Ag_2O−SnS_2 and CuO−SnS_2 structures are chemisorbed for NH_3, Cl_2, and C_2H_2 gases. From a moderate adsorption distance, large adsorption energy, charge transfer, and frontier molecular orbital theory analysis, different gas molecules' adsorption will induce changes in conductivity to different degrees. As a result, Ag_2O−SnS_2 is suitable for the NH_3 gas sensor, while CuO−SnS_2 is suitable for the C_2H_2 gas sensor. Under the doping of Ag_2O and CuO, the adsorption process mechanism and adsorption capacity are slightly different, but the adsorption of NH_3, Cl_2, and C_2H_2 is consistent. Ag_2O and CuO-modified SnS_2 is a suitable gas sensor and has a promising application in greenhouse cultivation.

AUTHOR INFORMATION

Corresponding Authors

Jingcheng Liu − *College of Electronic Information Engineering, Chongqing Technology and Business Institute, Chongqing 400052, China; Liquor Making Microbial Application & Detection Technology of Luzhou Key Laboratory, Luzhou Vocational & Technical College, Luzhou 646000, China*; Email: liujingcheng1980@126.com

Yingang Gui − *College of Engineering and Technology, Southwest University, Chongqing 400715, China*; orcid.org/0000-0001-8924-9379; Email: yinganggui@outlook.com

Authors

Wei Gong − *College of Electronic Information Engineering, Chongqing Technology and Business Institute, Chongqing 400052, China*

Heqing Huang − *College of Electronic Information Engineering, Chongqing Technology and Business Institute, Chongqing 400052, China*

Complete contact information is available at: https://pubs.acs.org/10.1021/acsomega.2c01828

Notes

The authors declare no competing financial interest.

ACKNOWLEDGMENTS

This work was funded by the Office of Science & Technology and Talent Work of Luzhou (2021-JYJ-92), Chongqing Technology and Business Institute project (ZZ2020-06).

REFERENCES

(1) Xie, Y.; Ruan, J.; Shi, Y.; Jin, S.; Tian, Y.; Zhu, L. Inversion detection method for resistivity of oil-immersed paper in transformer. *IEEE Trans. Power Delivery* **2019**, *34*, 1757−1765.

https://doi.org/10.1021/acsomega.2c01828
ACS Omega 2022, 7, 21043−21051

(2) Zhang, X.; Gui, Y.; Xiao, H.; Zhang, Y. Analysis of adsorption properties of typical partial discharge gases on Ni-SWCNTs using density functional theory. *Appl. Surf. Sci.* **2016**, *379*, 47−54.
(3) Lin, M.-J.; Chen, L.-B.; Yu, C.-T. A methodology for diagnosing faults in oil-immersed power transformers based on minimizing the maintenance cost. *IEEE Access* **2020**, *8*, 209570−209578.
(4) Liu, J.; Fan, X.; Zhang, Y.; Zheng, H.; Zhang, C. Condition prediction for oil-immersed cellulose insulation in field transformer using fitting fingerprint database. *IEEE Trans. Dielectr. Electr. Insul.* **2020**, *27*, 279−287.
(5) Chu, J.; Li, W.; Yang, X.; Wu, Y.; Wang, D.; Yang, A.; Yuan, H.; Wang, X.; Li, Y.; Rong, M. Identification of gas mixtures via sensor array combining with neural networks. *Sens. Actuators, B* **2021**, *329*, 129090.
(6) Zhang, X.; Yu, L.; Gui, Y.; Hu, W. First-principles study of SF_6 decomposed gas adsorbed on Au-decorated graphene. *Appl. Surf. Sci.* **2016**, *367*, 259−269.
(7) Zhang, X.; Yu, L.; Wu, X.; Hu, W. Experimental sensing and density functional theory study of H_2S and SOF_2 adsorption on Au-modified graphene. *Adv. Sci.* **2015**, *2*, 1500101.
(8) Cho, B.-N.; Chino, H.; Tsuji, H.; Kunito, T.; Makishima, H.; Uchida, H.; Matsumoto, S.; Oyaizu, H. Analysis of oil components and hydrocarbon-utilizing microorganisms during laboratory-scale bioremediation of oil-contaminated soil of kuwait. *Chemosphere* **1997**, *35*, 1613−1621.
(9) Verma, A. M.; Agrawal, K.; Kawale, H. D.; Kishore, N. Production of toluene by decomposition of 2-Hydroxy-6-methylbenzaldehyde: A DFT Study. *Chemistryselect* **2018**, *3*, 220−229.
(10) Gui, Y.; Li, T.; He, X.; Ding, Z.; Yang, P. Pt cluster modified h-BN for gas sensing and adsorption of dissolved gases in transformer oil: A Density Functional Theory Study. *Nanomaterials* **2019**, *9*, 1746.
(11) He, X.; Gui, Y.; Xie, J.; Liu, X.; Wang, Q.; Tang, C. A DFT study of dissolved gas (C_2H_2, H_2, CH_4) detection in oil on CuO-modified BNNT. *Appl. Surf. Sci.* **2020**, *500*, 144030.
(12) Gui, Y.; Peng, X.; Liu, K.; Ding, Z. Adsorption of C_2H_2, CH_4 and CO on Mn-doped graphene: Atomic, electronic, and gas-sensing properties. *Phys. E* **2020**, *119*, 113959.
(13) Chen, W.; Gui, Y.; Li, T.; Zeng, H.; Xu, L.; Ding, Z. Gas-sensing properties and mechanism of Pd-GaNNTs for air decomposition products in ring main unit. *Appl. Surf. Sci.* **2020**, *531*, 147293.
(14) Zhou, Q.; Zeng, W.; Chen, W.; Xu, L.; Kumar, R.; Umar, A. High sensitive and low-concentration sulfur dioxide (SO_2) gas sensor application of heterostructure NiO-ZnO nanodisks. *Sens. Actuators, B* **2019**, *298*, 126870.
(15) Wang, J.; Zhou, Q.; Xu, L.; Gao, X.; Zeng, W. Gas sensing mechanism of dissolved gases in transformer oil on Ag-MoS_2 monolayer: A DFT study. *Phys. E* **2020**, *118*, 113947.
(16) Leonardi, S. G.; Wlodarski, W.; Li, Y.; Donato, N.; Bonavita, A.; Neri, G. Ammonia sensing properties of two-dimensional tin disulphide/tin oxides (SnS_2/SnO_{2-x}) mixed phases. *J. Alloys Compd.* **2019**, *781*, 440−449.
(17) Hao, J.; Zhang, D.; Sun, Q.; Zheng, S.; Sun, J.; Wang, Y. Hierarchical SnS_2/SnO_2 Nanoheterojunctions with Increased Active-Sites and Charge Transfer for Ultrasensitive NO_2 Detection. *Nanoscale* **2018**, *10*, 7210−7217.
(18) Gui, Y.; Zhang, X.; Lv, P.; Wang, S.; Tang, C.; Zhou, Q. Ni-CNT chemical sensor for SF_6 decomposition components detection: A combined experimental and theoretical study. *Sensors* **2018**, *18*, 3493.
(19) Keshtkar, S.; Rashidi, A.; Kooti, M.; Askarieh, M.; Pourhashem, S.; Ghasemy, E.; Izadi, N. A novel highly sensitive and selective H_2S gas sensor at low temperatures based on SnO_2 quantum dots-C_{60} nanohybrid: Experimental and theory study. *Talanta* **2018**, *188*, 531−539.
(20) Ji, S.; Yang, J.; Xu, C.; Wang, J.; Xue, J. Temperature-programmed desorption/pulse surface reaction (TPD/TPSR) studies of CH_4, C_2H_6, C_2H_4, and CO over a cobalt/MWNTS catalyst. *React. Kinet. Catal. Lett.* **2006**, *89*, 209−217.
(21) Shin, H.; Krogel, J. T.; Gasperich, K.; Kent, P. R. C.; Benali, A.; Heinonen, O. Optimized structure and electronic band gap of monolayer GeSe from quantum monte carlo methods. *Phys. Rev. Mater.* **2021**, *5*, 024002.
(22) Liu, L.; Yang, Q.; Wang, Z.; Ye, H.; Chen, X.; Fan, X.; Zhang, G. High selective gas detection for small molecules based on germanium selenide monolayer. *Appl. Surf. Sci.* **2018**, *433*, 575−581.
(23) Wang, Y.; Li, T.; Peng, Y.; Gui, Y.; Sun, H. Pd and Pt decorated GeSe monolayers as promising materials for SOF_2 and SO_2F_2 sensing. *Appl. Surf. Sci.* **2021**, *560*, 150028.
(24) Li, X.; Tang, C.; Wang, J.; Tian, W.; Hu, D. Analysis and mechanism of adsorption of naphthenic mineral oil, water, formic acid, carbon dioxide, and methane on meta-aramid insulation paper. *J. Mater. Sci.* **2019**, *54*, 8556−8570.
(25) Wang, X.; Tan, J.; Han, C.; Wang, J.-J.; Lu, L.; Du, H.; Jia, C.-L.; Deringer, V. L.; Zhou, J.; Zhang, W. Sub-angstrom characterization of the structural origin for high in-plane anisotropy in 2D GeS_2. *ACS Nano* **2020**, *14*, 4456−4462.
(26) He, X.; Gui, Y.; Liu, K.; Xu, L. Comparison of sensing and electronic properties of C_2H_2 on different transition metal oxide nanoparticles (Fe_2O_3, NiO, TiO_2) modified BNNT (10,0). *Appl. Surf. Sci.* **2020**, *521*, 146463.
(27) Cao, W.; Gui, Y.; Chen, T.; Xu, L.; Ding, Z. Adsorption and gas-sensing properties of Pt_2-GaNNTs for SF_6 decomposition products. *Appl. Surf. Sci.* **2020**, *524*, 146570.
(28) Li, T.; Gui, Y.; Zhao, W.; Tang, C.; Dong, X. Palladium modified MoS_2 monolayer for adsorption and scavenging of SF_6 decomposition products: A DFT study. *Phys. E* **2020**, *123*, 114178.
(29) Gui, Y.; Shi, J.; Yang, P.; Li, T.; Tang, C.; Xu, L. Platinum modified MoS_2 monolayer for adsorption and gas sensing of SF_6 decomposition products: A DFT study. *High Voltage* **2020**, *5*, 454−462.
(30) Xu, L.; Gui, Y.; Li, W.; Li, Q.; Chen, X. Gas-sensing properties of Pt_n-doped WSe_2 to SF_6 decomposition products. *J. Ind. Eng. Chem.* **2021**, *97*, 452−459.
(31) Capelle, K.; Gross, E. K. U. Spin-density functionals from current-density functional theory and vice versa: A road towards new approximations. *Phys. Rev. Lett.* **1997**, *78*, 1872−1875.
(32) Gui, Y.; Shi, J.; Xu, L.; Ran, L.; Chen, X. Au-n (n=1-4) cluster doped $MoSe_2$ nanosheet as a promising gas-sensing material for C_2H_4 gas in oil-immersed transformer. *Appl. Surf. Sci.* **2021**, *541*, 148356.
(33) Wang, J.; Zhou, Q.; Zeng, W. Competitive adsorption of SF_6 decompositions on Ni-doped ZnO (100) surface: Computational and experimental study. *Appl. Surf. Sci.* **2019**, *479*, 185−197.
(34) Zheng, W.; Tang, C.; Xie, J.; Gui, Y. Micro-scale effects of nano-SiO_2 modification with silane coupling agents on the cellulose/nano-SiO_2 interface. *Nanotechnology* **2019**, *30*, 445701.
(35) Saidi, W. A.; Feng, H.; Fichthorn, K. A. Binding of polyvinylpyrrolidone to Ag surfaces: Insight into a structure-directing agent from dispersion-corrected density functional theory. *J. Phys. Chem. C* **2013**, *117*, 1163−1171.
(36) Delley, B. From molecules to solids with the DMol(3) approach. *J. Chem. Phys.* **2000**, *113*, 7756−7764.
(37) Perdew, J. P.; Burke, K.; Ernzerhof, M. Comment on "Generalized gradient approximation made simple" - Reply. *Phys. Rev. Lett.* **1998**, *80*, 891.
(38) Perdew, J. P.; Burke, K.; Ernzerhof, M. Generalized gradient approximation made simple. *Phys. Rev. Lett.* **1997**, *78*, 1396.
(39) White, J. A.; Bird, D. M. Implementation of gradient-corrected exchange-correlation potentials in car-parrinello total-energy calculations. *Phys. Rev. B* **1994**, *50*, 4954−4957.
(40) Delley, B. An all-electron numerical-method for solving the local density functional for polyatomic-molecules. *J. Chem. Phys.* **1990**, *92*, 508−517.
(41) Lu, J.; Zhang, Z. Convergence analysis of generalized nonlinear inexact uzawa algorithm for stabilized saddle point problems. *Front. Math. China* **2011**, *6*, 473−492.
(42) Gustafsson, B. The convergence rate for difference approximations to general mixed initial boundary-value-problems. *SIAM J. Numer. Anal.* **1981**, *18*, 179−190.
(43) Liu, S. H.; Tsai, H. M.; Pao, C. W.; Chiou, J. W.; Ling, D. C.; Pong, W. F.; Tsai, M. H.; Lin, H. J.; Jang, L. Y.; Lee, J. F.; Hsu, J. H.;

https://doi.org/10.1021/acsomega.2c01828
ACS Omega 2022, 7, 21043−21051

Wan, g W. J.; Hsu, C. J. Electronic and magnetic properties of the Ag-doped Fe_3O_4 films studied by x-ray absorption spectroscopy. *Appl. Phys. Lett.* **2006**, *89*, 092112.
(44) Cui, J.; He, J.; Chen, Y. Delocalized carriers and the electrical transport properties of n-Type GeSe crystals. *ACS Appl. Energy Mater.* **2019**, *2*, 3703−3707.
(45) van der Maelen, J. F.; Ruiz, J. Ag_2O versus Cu_2O in the Catalytic Isomerization of Coordinated Diaminocarbenes to Formamidines: A Theoretical Study. *Materials* **2022**, *15*, 491.
(46) Galliez, K.; Deniard, P.; Payen, C.; Lambertin, D.; Bart, F.; Koo, H.-J.; Whangbo, M.-H.; Jobic, S. Pair Distribution Function and Density Functional Theory Analyses of Hydrogen Trapping by gamma-MnO_2. *Inorg. Chem.* **2015**, *54*, 1194−1196.
(47) Tavakol, H.; Shahabi, D. DFT, QTAIM, and NBO Study of Adsorption of Rare Gases into and on the Surface of Sulfur-Doped, Single-Wall Carbon Nanotubes. *J. Phys. Chem. C* **2015**, *119*, 6502−6510.
(48) Tavakol, H.; Shahabi, D.; Keshavarzipour, F.; Hashemi, F. Theoretical calculation of simple and doped CNTs with the potential adsorption of various ions for water desalination technologies. *Struct. Chem.* **2020**, *31*, 399−409.
(49) Mananghaya, M.; Yu, D.; Yu, D.; Santos, G. N.; Rodulfo, E. Adsorption of Mercury(II) Chloride and Carbon Dioxide on Graphene/Calcium Oxide (0 0 1). *Korean J. Mater. Res.* **2016**, *26*, 298−305.
(50) Mananghaya, M. R. Adsorption of CO and desorption of CO_2 interacting with Pt (111) surface: a combined density functional theory and Kinetic Monte Carlo simulation. *Adsorption* **2020**, *26*, 461−469.

https://doi.org/10.1021/acsomega.2c01828
ACS Omega 2022, 7, 21043−21051